Cavity-enhanced second harmonic generation in a silica whispering-gallery microresonator

June 9, 2017

Centrosymmetric materials ... most significant application: surface probe... surface response is intrinsically weak, so several methods are used to enhanced surface SHG (e.g. plasmonic)... cavity boosts the intensity of light, making it a good platform for nonlinear optics...cavity enhanced SHG... Recently, SHG with bare silica cavity (Asano OL)...

Here, second harmonic, originating from symmetry breaking at the surface and bulk multipole response (fig.1 **b**), is observed under the continuous wave pump below 1 mW in a WGM microsphere made of centrosymmetric material. An unprecedented conversion efficiency of 0.049% W^{-1} benefits from doubly resonant enhancement of ultrahigh Q modes (phase-matching condition[also know as perfect phase matched]), which is achieved by dispersion engineering including thermal effect, optical Kerr effect and geometric control of cavity.

The work enriches the nonlinear toolbox of silica/silicon photonics and largely extends the emission range of silica microresonators under low pump power (below 1 mW), making it possible to push the frequency conversion process down to the quantum regime[refs in Asano OL]. More significantly, the fruitful surface SHG and SFG detection methods can be introduced into (bridged with?) the sensitive microcavity sensing, which enables surface-specific detection with low pump power and high sensitivity.

In the experiment, a silica microsphere (diameter ~ 62 μm) is pumped through a tapered optical fiber (waist diameter around 1 μm) at 1550 nm band [1, 2], as shown in fig.1 **a**. To collect SH signal efficiently, a second fiber taper (waist diameter around 0.5 μm) designed for 780 nm band is incorporated into the system. The intrinsic quality factor (Q) for the pumped cavity mode is 4.8×10^7. Figure 1**c** shows a typical SH spectrum from the electron-multiplying CCD (EMCCD) and the corresponding pump spectrum from the optical spectrum analyzer (OSA). The SH signal of 777.75 nm appears when pumped at 1555.14 nm, which deviates only 0.023% from the expected wavelength, falling into the resolution tolerance of OSA and EMCCD. Note that stimulated Raman scattering and parametric oscillation do not occur because their thresholds are above the pump power in the experimentThird harmonic generation is also absent due to the phase mismatch in the nonlinear optical process. Moreover, SH signals arise in the full range when cavity modes are pumped from 1545 nm to 1565 nm, as shown in Fig.1d. Among the occurrence of SH, a maximum signal power of 5 nW can be obtained via the signal fiber. In comparison of the collecting efficiency of the two fibers, the fiber-cavity coupling is optimized so that the SH signal from the pump fiber is observable but the maximum power is over one order of magnitude weaker than the power from the signal fiber. From either fibers, SH signal is absent when the pump is off-resonance with cavity modes, which helps to eliminate the possibility of spurious signals such as the second order diffraction of the EMCCD grating.

The dependence of SH power on pump power can be derived from coupled mode equations[3].

$$P_2 = \frac{4|g|^2 Q_2 \eta_2/\omega_2}{4Q_2^2(2\omega_p/\omega_2 - 1)^2 + 1} \frac{16 Q_1^2 \eta_1^2 P_1^2/\omega_1^2}{[4Q_1^2(\omega_p/\omega_1 - 1)^2 + 1]^2}, \tag{1}$$

where the subscripts 1, 2 represent the pumped mode and SH mode respectively. P_i $(i = 1, 2)$is the power in the corresponding tapered fiber near the microsphere, g is a coupling coefficient between two modes, which will be looked into in the next section. Q_i is the total quality factor, ω_i is the mode frequency and ω_p is the pump frequency. $\eta_i = Q_i/Q_{ie}$ is the coupling factor and Q_{ie} is the external quality factor. The pump power depletion is ignored due to the weak second order nonlinear effect in silica. The enhancement of SH power by ultrahigh-Q microresonator is obvious in eq.(1).

Achieving phase-matching condition lies in the heart of the doubly resonant enhancement of second order effects and reaching the high conversion efficiency. The ultrahigh Q represents the factor of enhancement but also presents a challenge to phase matching or double resonance in a microresonator[4, 5, 6, 7]($\omega_p = \omega_1, 2\omega_p = \omega_2$). SH modes with higher order radial number have been proposed or used to compensate the material and geometric dispersion[5]. For SHG, a silica microsphere with a diameter of 60 μm gives rise to good phase-matching between a fundamental mode near 1550 nm and an SH mode with radial number $q_2 = 2$ (see Supplementary Information). In the experiment, the desired phase-matching can be disturbed by the deviation of cavity from its designed geometry, making one of the mode off-resonance and impeding highly efficient SHG. Therefore, the cavity dispersion should be finely adjusted to compensate the deviation, where mode frequency shift induced by thermal behavior (namely thermal expansion, thermally induced refractive index change and the optical Kerr effect) can be a versatile tool to achieve the goal[8, 9].

The mechanism of thermal and Kerr assisted phase matching process is explained in fig.2a. When the pump power is weak and the mode frequency shift is negligible (cold cavity), the pumped and SH modes even with higher radial order usually cannot be on resonance with the pump light and its SH simultaneously. Increasing the input power leads to the appearance and broadening of

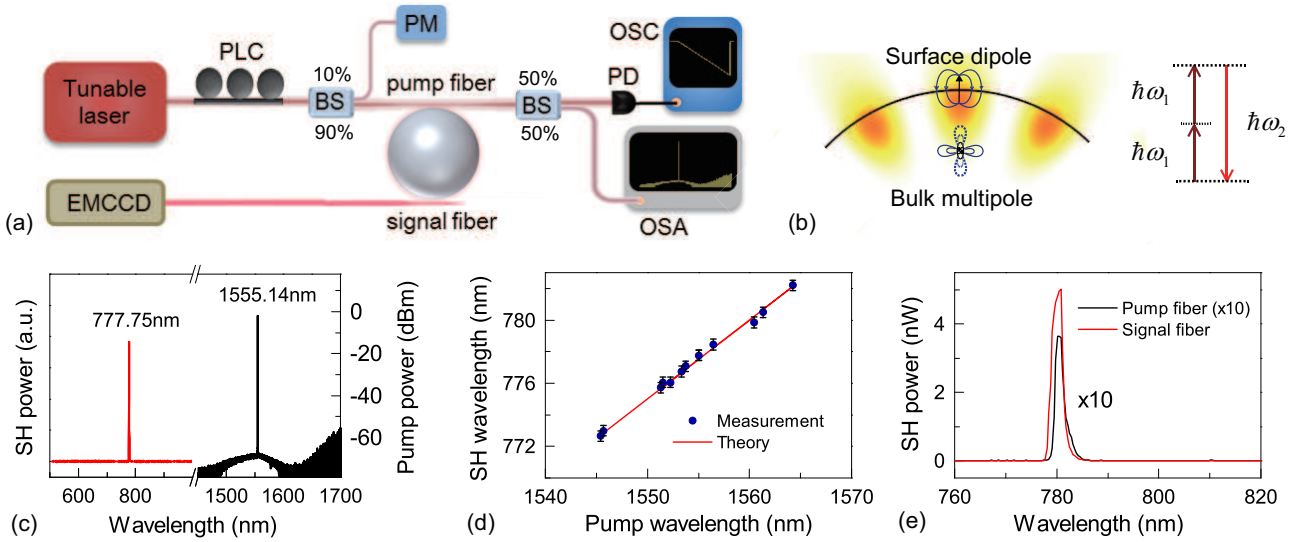

Figure 1: **Experimental set-up and observation of cavity-enhanced SH signals. a,** The pump light from a tunable laser around 1550 nm is coupled into a silica microsphere through a tapered fiber, and a second fiber is used to collect the SH signal. OSC: oscilloscope. OSA: optical spectrum analyzer. PLC: polarization controller. BS: beam splitter. EMCCD: electron-multiplying CCD. **b,** SH is generated from the surface dipole response and the bulk multipole response in a WG microsphere. **c,** Measured SH spectrum (red) and the corresponding pump spectrum (black). **d,** Measured SH wavelengths versus the corresponding pump wavelengths when different modes are pumped. **e,** Comparison of SH power collected by signal fiber and pump fiber (10 times magnified).

the non-Lorentzian, triangular transmission shape for the pump[10]. The SH mode also experiences a red shift from cold cavity frequency and the rate of red shift is different for the SH of pump light and the SH mode, making it possible for them to be on resonance in the process of tuning the pump frequency. At the on-resonance pump frequency for SH, the phase-matching condition is fulfilled and the SH power reaches a peak value (corresponding to state 2 in fig.2a and b). Due to the ultrahigh Q of the SH resonance, the SH power diminishes rapidly before and after reaching the on-resonance pump frequency (state 1 and 3 in fig.2a and b). The SH signal is much weaker than the pump so that its thermal and Kerr effects are negligible in this process. As shown in fig. 2c, the SH power is measured by varying the pump wavelength in the detuning range of the gray area in fig. 2b with a fixed input power of 4.46 mW. [fitting results here]

[The red shift of the SH mode is proportional to the intra-cavity power, which is proportional to the pump light detuning from the cold cavity frequency. It means $\Delta\omega_2 = D_{12}\Delta\omega_p$, where $\Delta\omega_2$ is the SH mode frequency shift, $\Delta\omega_p$ is the pump light detuning and D_{12} is the proportionality coefficient. Using this relation and eq.(1), the experimental parameters can be fit by the theory to be $Q_2 \times (2 - D_{12}) = 8.57 \times 10^5$.]

The dependence of SH power on power pump is also measured, as shown in fig.2d. At each input power, we search for the maximum SH output power in the wavelength range from the cold cavity mode (1555.02nm) to the pump on-resonance wavelength. Among different values of input power, a critical power manifests itself, at which the SH power reaches the peak value just before the pump light becomes on resonance and then thermally unlocked. In this case, the pump light and its SH achieve double resonance simultaneously, which represents the most efficient SHG with the pump power of 879 μW and the conversion efficiency of 0.049% W^{-1}. Below the critical input power, the SH of pump light is off resonance when the pump is still thermally locked in the mode, which largely weakens the SH power. Above the critical power, the increasing input power shifts the pumped mode more to the red side (the pump is not completely on resonance) and lowers the enhancement of the pump light, which counteracts with the increasing input power and makes the intracavity power almost unchanged at the SH resonant detuning. Consequently, the SH power remains the same with increasing input power.

[Fitting] The critical input power is fitted to be 832.5μW and the corresponding SH power is fitted to be 381pW. Eq.(1) and $\omega_1 = \omega_{10} - B_{11}|\alpha_1|^2$ [10], $\omega_2 = \omega_{20} - B_{12}|\alpha_1|^2$ are used to fit the experimental data, where ω_{i0} is the mode frequency in the cold cavity, $|\alpha_1|^2$ is normalized to the intra-cavity power of the pumped mode and B_{1i} is the coefficient of intra-cavity power induced frequency shift. The parameters related to the pumped mode can be extracted from the measurements.

[where?] In the THG experiments in silica microresonators[4, 7], the phase mismatch curve is flat for high order radial modes, and the shift speed of the pump TH frequency and the TH frequency mode may be similar. Consequently, the high order radial modes induced phase matching may play a major role so that the P_1^3 relation can be observed. Microresonator SHG in other materials usually use different phase matching strategy to achieve broad band or tunable phase matching, e.g. quasi-phase-matching [cite more later]...The quality factor is also moderate so that the thermal effect and Kerr effect do not manifest themselves in the SHG process.

It is also possible to measure the explicit $P_2 \propto P_1^2$ dependence by introducing another degree of freedom to

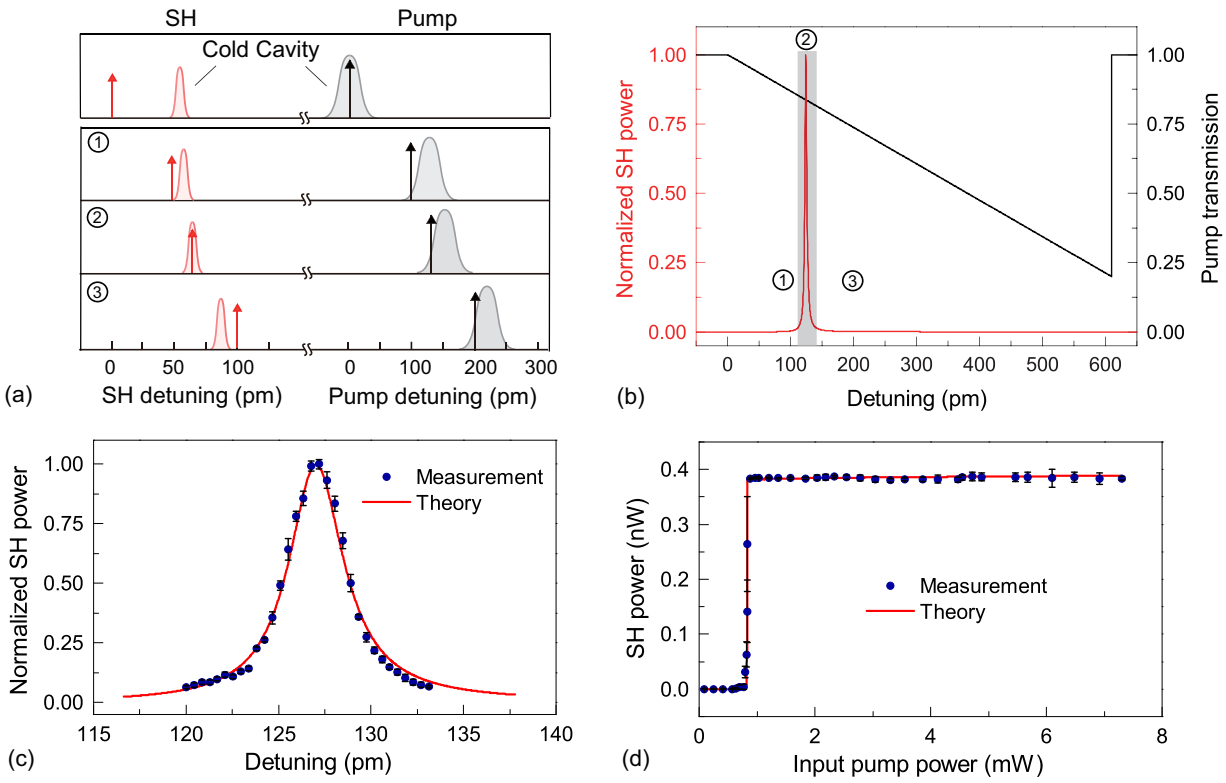

Figure 2: **Thermal effect and Kerr effect assisted phase-matching.** **a,** Schematic of the phase-matching process. Detuning here is the wavelength relative to the cold-cavity wavelength of the pumped mode (to half of this wavelength for SH detuning). The black (red) arrow represents the detuning of the pump light (its SH). The gray (red) Lorentzian line represents the pumped mode (SH mode). 1-3 show three states with increasing pump wavelength but the same input power. **b,** Normalized SH power and the pump transmission at different pump wavelength detuning. 1-3 correspond to the three states in panel **a**. The gray area is enlarged in panel **c** as the theoretical red line. **c,** SH power versus pump detuning with the input power of 4.46mW. **d,** The dependence of maximum SH power at all the pump detuning on the input power.

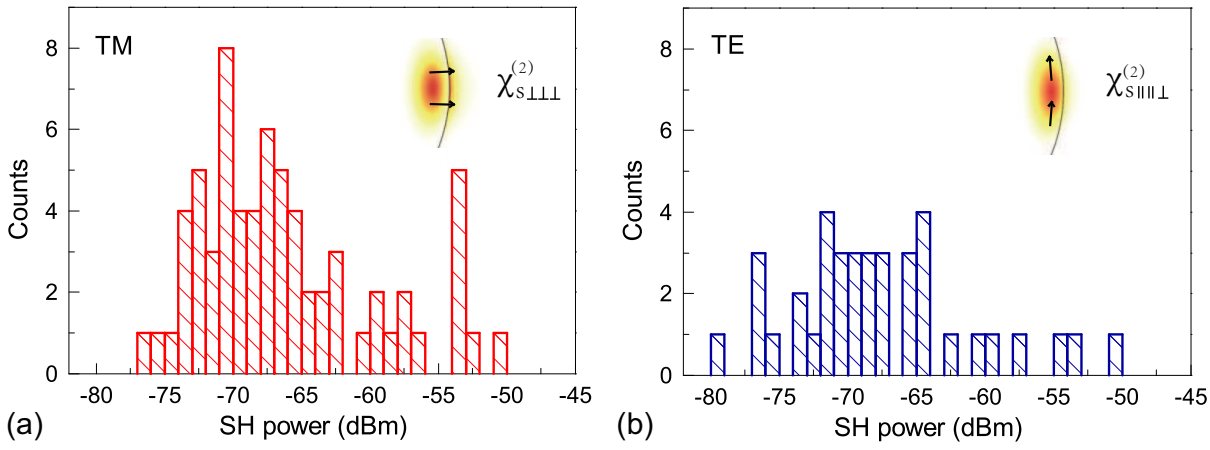

Figure 3: **SH power histogram with different pump polarization.** **a,** TM and **b,** TE modes are pumped to generate SH respectively. Insets: Field amplitude distribution and the direction of the electric field (black arrow).

manipulate the SH mode frequency. For example, a control light can be coupled into another mode to change the intra-cavity power and thus achieving the double on-resonance condition at various input pump power. The specific measurement plan is beyond the scope of this [letter?] and is still under investigation.

Apart from the unique power dependence, the SH power enhanced by the microresonator also exhibits a polarization dependence. The polarization of the pump light is adjusted so that transverse magnetic (TM) or trans-

verse electric (TE) modes from 1545 nm to 1565 nm are pumped. The maximum SH power of each SHG process is recorded for the two polarization respectively, as shown in the histogram in 3. After searching for SH in the wavelength range three times with each polarization, a total number of 69 (40) SHG incidence is recorded for TM (TE) polarization, and the average SH power is 0.843 nW (0.619 nW). The dependence on polarization originates from the polarization dependent nonlinear coupling coefficient g in eq.(1), which bridges the microresonator with the second order nonlinearity of centrosymmetric material.

Using the Helmholtz equation and the relation between electric field and nonlinear polarization, the coupling coefficient induced by surface nonlinear response can be derived as

$$g_{s0} = 2i\frac{\omega_1^2}{\omega_2 n^2}\frac{\int_{\text{surface}} \mathbf{E}_{02}^* : \chi_{s0}^{(2)} : \mathbf{E}_{01}\mathbf{E}_{01}\mathrm{d}\mathbf{S}}{\int |\mathbf{E}_{02}|^2 \mathrm{d}\mathbf{V}} \qquad (2)$$

where n is the refractive index, $\chi_s^{(2)}$ is the surface nonlinear susceptibility, and $\mathbf{E}_{0i}(\mathbf{x})$ is the normalized electric field so that $\alpha_i\mathbf{E}_{0i}(\mathbf{x})$ represents the complete electric field.

The bulk multipole nonlinear polarization can be written as $\mathbf{P}_\gamma = \gamma\nabla(\mathbf{E}\cdot\mathbf{E})$ and $\mathbf{P}_\delta = \delta(\mathbf{E}\cdot\nabla)\mathbf{E}$, where γ and δ are the nonlinear coefficients. The first term represents a longitudinal wave and can couple with the SH only at the surface. Therefore it can be incorporated into an effective surface susceptibility $\chi_s^{(2)} = \chi_{s0}^{(2)} + \chi_{s,\gamma}^{(2)}$[11]. The coupling coefficient induced by the second term can be written as

$$g_b = 2i\frac{\omega_1^2}{\omega_2 n^2}\frac{\int \delta\mathbf{E}_{02}^* \cdot (\mathbf{E}_{01}\cdot\nabla)\mathbf{E}_{01}\mathrm{d}\mathbf{V}}{\int |\mathbf{E}_{02}|^2 \mathrm{d}\mathbf{V}} \qquad (3)$$

The total coupling coefficient between the two modes is $g = g_s + g_b$.

There are three non-zero components $\chi_{\perp\perp\perp}$, $\chi_{\parallel\parallel\perp}$ and $\chi_{\perp\parallel\parallel}$ in the surface second order susceptibility tensor of fused silica. $\chi_{\perp\perp\perp}$ ($\chi_{\parallel\parallel\perp}$) plays a major role when TM (TE) mode is pumped. $\chi_{\perp\parallel\parallel}$ can be ignored in studying SHG due to the non-degeneracy of TM and TE modes. TM modes are preferable in surface induced SHG because $\chi_{\perp\perp\perp}$ is nearly an order of magnitude larger than $\chi_{\parallel\parallel\perp}$ [12]. The amplitude of bulk nonlinear response g_b relies on the specific field distribution in the microsphere. Note that for a TE mode, the divergence is along the polar direction, which exhibits geometric symmetry with regard to the equatorial plane. If both the pumped mode and the SH mode are fundamental in the polar direction (polar number l = azimuthal number m), g_b vanishes due to the divergence and the polar symmetry. Because of a better confinement in the radial direction and thus a larger divergence for most of the modes, TM modes tend to have a larger g_b than TE modes. For example, in a silica microsphere with a diameter of 62μm, the TM pumped mode with $l_1 = m_1 = 171$ and its SH mode with $l_2 = m_2 = 342$ produces a g_b 18 times larger than that of the TE mode with $l_1 - 1 = m_1 = 171$ and its SH mode with $l_2 - 1 = m_2 = 342$ (in both cases, the radial numbers of the pumped mode and SH mode are 1 and 2 respectively due to phase matching considerations).

The polarization dependence can be utilized to add to the surface specificity for SHG sensing. Mediated by $\chi_{\parallel\parallel\perp}$, two TE polarized photons can generate a TM polarized photon. For nonlinearity from bulk multipole effects (g_b), TE polarized pump can only generate TE SH. In this case, the bulk response can be eliminated and thus restricting the SHG on the surface.

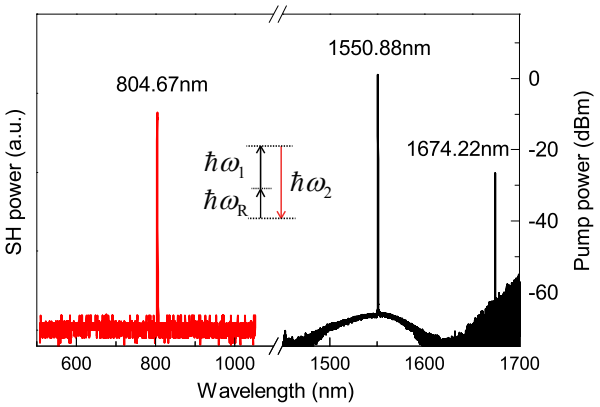

Figure 4: **Measured spectra of second-order sum frequency generation (SFG).** The pump light (ω_1) and Raman light (ω_2) are summed to generate the SF signal (ω_3).

Sum frequency generation (SFG) can also take place when the pumped mode produce a Raman signal. Shown in fig.4b is an SF signal (804.67 nm) and the corresponding pump (1550.88 nm) and its Raman signal (1674.22 nm) with an input power of 7.33 mW, which is above the Raman threshold for this mode. The deviation of the SF wavelength from the expected value (804.63 nm) is much smaller than the resolution of EMCCD.

[Conclusion]

References

[1] J Cheung Knight, G Cheung, F Jacques, and TA Birks. Phase-matched excitation of whispering-gallery-mode resonances by a fiber taper. *Optics letters*, 22(15):1129–1131, 1997.

[2] Ming Cai, Oskar Painter, and Kerry J Vahala. Observation of critical coupling in a fiber taper to a silica-microsphere whispering-gallery mode system. *Physical review letters*, 85(1):74, 2000.

[3] Hermann A Haus and Weiping Huang. Coupled-mode theory. *Proceedings of the IEEE*, 79(10):1505–1518, 1991.

[4] Tal Carmon and Kerry J Vahala. Visible continuous emission from a silica microphotonic device by third-harmonic generation. *Nature Physics*, 3(6):430–435, 2007.

[5] Gregory Kozyreff, JL Dominguez Juarez, and Jordi Martorell. Whispering-gallery-mode phase matching for surface second-order nonlinear optical processes in spherical microresonators. *Physical Review A*, 77(4):043817, 2008.

[6] Yong Xu, Ming Han, Anbo Wang, Zhiwen Liu, and James R Heflin. Second order parametric processes in nonlinear silica microspheres. *Physical review letters*, 100(16):163905, 2008.

[7] D Farnesi, A Barucci, GC Righini, S Berneschi, S Soria, and G Nunzi Conti. Optical frequency conversion in silica-whispering-gallery-mode microspherical resonators. *Physical review letters*, 112(9):093901, 2014.

[8] Pascal DelHaye, T Herr, E Gavartin, ML Gorodetsky, Ronald Holzwarth, and Tobias J Kippenberg. Octave spanning tunable frequency comb from a microresonator. *Physical Review Letters*, 107(6):063901, 2011.

[9] T Herr, V Brasch, JD Jost, CY Wang, NM Kondratiev, ML Gorodetsky, and TJ Kippenberg. Temporal solitons in optical microresonators. *Nature Photonics*, 8(2):145–152, 2014.

[10] Tal Carmon, Lan Yang, and Kerry J Vahala. Dynamical thermal behavior and thermal self-stability of microcavities. *Optics Express*, 12(20):4742–4750, 2004.

[11] Tony F Heinz. Second-order nonlinear optical effects at surfaces and interfaces. *Nonlinear surface electromagnetic phenomena*, 29, 1991.

[12] Francisco J Rodriguez, Fu Xiang Wang, and Martti Kauranen. Calibration of the second-order nonlinear optical susceptibility of surface and bulk of glass. *Optics express*, 16(12):8704–8710, 2008.